Quasiparticle band-structure calculations for C, Si, Ge, GaAs, and SiC using Gaussian-orbital basis sets

Michael Rohlfing, Peter Krüger, and Johannes Pollmann
Institut für Theoretische Physik II– Festkörperphysik, Universität Münster, D-48149 Münster, Germany
(Received 6 July 1993)

We report state-of-the-art first-principles calculations of the quasiparticle energies of prototype homopolar and heteropolar covalent semiconductors described in terms of the electron self-energy operator. The wave functions are calculated within density-functional theory using the local-density approximation and employing nonlocal, norm-conserving pseudopotentials. The self-energy operator is evaluated in the *GW* approximation. Employing the plasmon-pole approximation for the frequency dependence of the dielectric matrix $\epsilon_{G,G'}(\mathbf{q},\omega)$, its static part is fully calculated within the random-phase approximation (RPA) as well as by using a number of different models. All calculations are carried out employing localized Gaussian orbital basis sets. This will turn out to be very useful for detailed studies of the quasiparticle properties of more complex systems such as bulk defects including lattice relaxation and reconstructed surfaces with large unit cells or interfaces, which are otherwise computationally too demanding. Using an s,p,d,s^* basis set of 40 Gaussian orbitals for Si, for example, yields already convergent results in excellent agreement with the results of a 350-plane-wave calculation in the corresponding plane-wave representation. Most of our results for Si, diamond, Ge, and GaAs are in very good agreement with experimental data and with available plane-wave *GW* calculations. To our knowledge, our results for SiC are the first quasiparticle energies reported so far for this important material of high current technological interest. Also in this case we find very good agreement with the available experimental data except for $E(L_{1c})$. We believe that this deviation may be attributed to experimental uncertainties. In particular, we discuss and scrutinize the applicability of six different models for the static dielectric matrix $\epsilon_{G,G'}(\mathbf{q},0)$ in the *GW* approximation ranging from the simple Hartree-Fock expression over diagonal models to nondiagonal models that take the local fields within the inhomogeneous electronic charge density into account. Some of the nondiagonal models are shown to yield results in very good agreement with the full RPA results.

I. INTRODUCTION

The local-density approximation[1,2] (LDA) of density-functional theory (DFT) has been established as a very powerful tool for studying ground-state properties of bulk semiconductors, their surfaces, or interfaces, and of bulk defects in semiconductors from first principles.[3–5] The DFT provides an exact formulation for the ground-state energy. Excitation energies, however, do not directly follow from that theory, since the one-particle eigenvalues in LDA are not formally interpretable as quasiparticle energies. The failures of such interpretations are well known. Band gaps in semiconductors are typically underestimated by 30–50%, and in particular cases like Ge or ZnO the gap is closed[6] or nearly closed,[7] respectively. To remedy these failures in the calculated band gaps and, in particular, to calculate excited-state properties, direct quasiparticle band-structure calculations are required.

The basic formal development of first-principles methods for calculating the quasiparticle energies and excited-state properties of real materials were put forward more than two decades ago by Hedin and Lundqvist.[8,9] For semiconductors, the major difficulty stems from an adequate treatment of the dynamical correlations of the electrons in a solid with an energy gap and a strongly inhomogeneous charge density. The basic object of this theory is the nonlocal, non-Hermitian, and energy-dependent self-energy operator $\Sigma(\mathbf{r},\mathbf{r}',E)$. In lowest approximation, Σ is given as a product of the Green's function G times the screened Coulomb interaction W. This approximation is usually referred to as the *GW* approximation (GWA).[8,9] In their landmark contributions to the field, Hybertsen and Louie,[10] as well as Godby, Schlüter, and Sham[11] developed practicable schemes for evaluating the many-body corrections within the GWA, and arrived at theoretical results which showed excellent agreement with a whole body of experimental data. Three elements in the theory were found to be critical for the success: a proper account of the nonlocality of the Green's function G, the inclusion of the full dielectric matrix in the screened Coulomb interaction W, and an adequate treatment of dynamical effects in the screening. In the meantime a number of *GW* calculations have been reported which confirm the excellent agreement with experiment for many more semiconductors and insulators (see the references in Sec. II). A number of surfaces[12] and adsorbate systems[13] with not too large unit cells have been treated this way, yielding very good agreement with photoemission and inverse photoemission data as well.

One common feature of *GW* calculations that have

been carried out so far is that nearly all of them employ *plane-wave basis sets* (it should be noted that for some quasiparticle calculations, e.g., nickel[14] and C_{60},[15] localized basis sets have been employed as well). For bulk Si, e.g., about 350 plane waves were found to yield convergent results.[10] For Si and Ge surfaces calculated in the supercell geometry with 12 Si layers per supercell more than 2000 plane waves are needed. Obviously, if even more complex systems are to be addressed, the drastically increasing number of plane waves necessary for the basis set turns out to be one of the bottlenecks for such calculations. This problem can be overcome if localized basis sets of, e.g., Gaussian orbitals are used. Another bottleneck in the calculations can be the evaluation of the nonlocal dielectric matrix, which calls for many reciprocal lattice vectors in Fourier space if slabs or supercells are to be properly described. In this respect, appropriate model dielectric matrices that can be computed with modest numerical effort could turn out to be mandatory. The calculation of the dielectric matrix within the full random-phase approximation (RPA) is much more time consuming. It may turn out to be too demanding for very complex systems.

In order to provide a basis for manageable *GW* calculations of more complex systems such as semiconductor surfaces with large unit cells, semiconductor interfaces, or bulk defects including lattice relaxation, in this paper we report *GW* calculations for homopolar and heteropolar covalent bulk semiconductors using localized Gaussian-orbital basis sets. In addition to the full calculations of the respective static dielectric matrices within the RPA, we discuss a number of model dielectric functions and analyze their applicability within these calculations.

To be able to compare our results in a meaningful way with previous results, we have used nonlocal, norm-conserving pseudopotentials and the same exchange-correlation potential as in Ref. 10. We show that our calculations employing relatively small Gaussian-orbital basis sets yield essentially the same results as plane-wave calculations if both are carried out to basis-set convergence.

The paper is organized as follows. In Sec. II, we briefly summarize the basic equations of the GWA and point out how we calculate the static dielectric matrix within the RPA. In Sec. III, we present and discuss six different models for the static dielectric matrix which we have also used in our calculations. Some numerical details of our LDA and GWA calculations are given in Sec. IV. In Sec. V, we present and discuss the results of our studies for Si, Ge, GaAs, diamond, and SiC. To our knowledge, our quasiparticle band structure for SiC is the first GWA result for this material. In Sec. VI we address the electronic part of the static dielectric constant, ϵ_∞, as calculated from our RPA results for the static dielectric matrix. This quantity enters the model dielectric matrices of Sec. III, and it is interesting to analyze the differences in the quasiparticle band structures resulting when the calculated ϵ_∞ is used in the models instead of experimental values for ϵ_∞. A short summary concludes the paper in Sec. VII.

II. THE *GW* APPROXIMATION

A powerful technique for the calculation of the ground-state properties of semiconductors and insulators from first principles is given by the DFT-LDA. Its central aspect is the approximation of exchange-correlation effects by a potential $V_{\rm xc}(\mathbf{r})$ which depends on the local density $\rho(\mathbf{r})$. In the LDA one has to solve the Kohn-Sham equation

$$\left\{-\frac{\hbar^2}{2m}\nabla^2+\hat{V}_{\rm ps}(\mathbf{r})+e^2\int\frac{\rho(\mathbf{r}')}{|\mathbf{r}-\mathbf{r}'|}d^3r'+V_{\rm xc}(\rho(\mathbf{r}))\right\}\psi_{n\mathbf{k}}(\mathbf{r})=E_{n\mathbf{k}}^{\rm LDA}\psi_{n\mathbf{k}}(\mathbf{r})\ . \quad (1)$$

This equation is usually formulated only for the valence electrons. Therefore, the electron-ion interaction is described by a pseudopotential $\hat{V}_{\rm ps}$. This state-of-the-art method has been applied to many systems and the calculated ground-state properties, e.g., the theoretical lattice constant and theoretical bulk modulus agree well with experimental data.[3–5] Usually, the energylike Lagrangian parameters of (1), $E_{n\mathbf{k}}^{\rm LDA}$, are regarded as single-particle energies. This yields quite reliable band structures, at least for the valence-band states. Nevertheless, the LDA energy values are not exact single-particle energies. As mentioned already, all LDA band structures for semiconductors suffer from a fundamental gap that is too low. To obtain band structures that give reliable energy values for the conduction-band states as well, quasiparticle corrections have to be taken into account as they are given, e.g., by the *GW* approximation.

The principles of the *GW* approximation, as used in our work, have been exposed by many other authors,[8–11,16,17] and will be given here in the form of a brief summary only. The central quantity within this formalism is the single-particle Green's function[8,9]

$$G(\mathbf{r},\mathbf{r}',E)=\sum_{n\mathbf{k}\sigma}\frac{\psi_{n\mathbf{k}\sigma}(\mathbf{r})\psi_{n\mathbf{k}\sigma}^*(\mathbf{r}')}{E-E_{n\mathbf{k}\sigma}+i0^+\,\mathrm{sgn}(E_{n\mathbf{k}\sigma}-\mu)}\ . \quad (2)$$

The Green's function satisfies an equation which can be written in terms of one-particle wave functions as

$$\left\{-\frac{\hbar^2}{2m}\nabla^2+\hat{V}_{\rm ps}(\mathbf{r})+e^2\int\frac{\rho(\mathbf{r}')}{|\mathbf{r}-\mathbf{r}'|}d^3r'\right\}\psi_{n\mathbf{k}}(\mathbf{r})+\int\Sigma(\mathbf{r},\mathbf{r}',E_{n\mathbf{k}})\psi_{n\mathbf{k}}(\mathbf{r}')d^3r'=E_{n\mathbf{k}}\psi_{n\mathbf{k}}(\mathbf{r})\ . \quad (3)$$

Again, this equation is usually formulated for valence electrons only. As in the LDA, the electron-ion interaction is described by a pseudopotential $\hat{V}_{\rm ps}$. We use norm-conserving *ab initio* pseudopotentials throughout our work.

The central difficulty connected with Eq. (3) is to find an adequate approximation for the self-energy operator, $\Sigma(\mathbf{r},\mathbf{r}',E)$. Within the *GW* approximation, it is calculated from the Green's function G and the dynamically screened Coulomb interaction W:

$$\Sigma(\mathbf{r},\mathbf{r}',E)=\frac{i}{2\pi}\int e^{-i\omega 0^+}G(\mathbf{r},\mathbf{r}',E-\omega)W(\mathbf{r},\mathbf{r}',\omega)d\omega \ . \tag{4}$$

The screened interaction W can be written by introducing the inverse dielectric function. Within the Fourier representation, one obtains

$$W_{\mathbf{G},\mathbf{G}'}(\mathbf{q},\omega)=\epsilon^{-1}_{\mathbf{G},\mathbf{G}'}(\mathbf{q},\omega)\frac{4\pi e^2}{V}\frac{1}{|\mathbf{q}+\mathbf{G}|}\frac{1}{|\mathbf{q}+\mathbf{G}'|} \ . \tag{5}$$

Within the GW approximation, the dielectric function is calculated as follows:

$$\epsilon_{\mathbf{G},\mathbf{G}'}(\mathbf{q},\omega)=\delta_{\mathbf{G},\mathbf{G}'}+2\frac{4\pi e^2}{V}\frac{1}{|\mathbf{q}+\mathbf{G}|}\frac{1}{|\mathbf{q}+\mathbf{G}'|}\times\sum_{\mathbf{k}}\sum_{\substack{m\in VB\\ n\in CB}}\left[\int\psi^*_{m\mathbf{k}}(\mathbf{r})e^{-i(\mathbf{q}+\mathbf{G})\mathbf{r}}\psi_{n,\mathbf{k}+\mathbf{q}}(\mathbf{r})d^3r\right]\left[\int\psi^*_{m\mathbf{k}}(\mathbf{r})e^{-i(\mathbf{q}+\mathbf{G}')\mathbf{r}}\psi_{n,\mathbf{k}+\mathbf{q}}(\mathbf{r})d^3r\right]^*\times\left[\frac{1}{E_{n,\mathbf{k}+\mathbf{q}}-E_{m\mathbf{k}}-\omega+i0^+}+\frac{1}{E_{n,\mathbf{k}+\mathbf{q}}-E_{m\mathbf{k}}+\omega+i0^+}\right] \ . \tag{6}$$

The orthogonality of wave functions of different spins has been taken into account here. Equation (6) is the same result as obtained by the random-phase approximation (RPA). Before inserting into Eqs. (4) and (5), these matrices have to be inverted with respect to the reciprocal-lattice vectors $\mathbf{G}$ and $\mathbf{G}'$ to obtain the *inverse* dielectric matrices. It should be noted that time-ordered quantities instead of causal ones are required by the GW approximation. We calculate the dielectric matrices in the symmetric form, which is less difficult to evaluate.

In general, Eq. (3) has to be solved self-consistently with respect to the charge density $\rho(\mathbf{r})$ and the quasiparticle energies $E_{n\mathbf{k}}$. Usually, the self-energy operator is calculated approximately by taking the wave functions $\psi_{n\mathbf{k}}(\mathbf{r})$ and the band-structure energies $E_{n\mathbf{k}}$ from the LDA. Thus both the Green's function G and the dielectric function ϵ are calculated from the respective LDA results. In the solution of Eq. (3), it turned out, e.g., for Si,[10] that the eigenfunctions $\psi_{n\mathbf{k}}(\mathbf{r})$ are very similar to the LDA eigenfunctions $\psi^{\mathrm{LDA}}_{n\mathbf{k}}(\mathbf{r})$. We therefore assume this behavior for the systems studied in this paper, as well (the index LDA at the wave functions therefore will be omitted from now on). Taking into account that the wave functions satisfy the Kohn-Sham equation (1), from (1) and (3) one obtains as a great simplification the relation

$$E_{m\mathbf{k}}=E^{\mathrm{LDA}}_{m\mathbf{k}}+\langle\psi_{m\mathbf{k}}|\Sigma(E_{m\mathbf{k}})-V_{\mathrm{xc}}|\psi_{m\mathbf{k}}\rangle \ . \tag{7}$$

According to this equation, the LDA energy values $E^{\mathrm{LDA}}_{m\mathbf{k}}$ are corrected by the GW approximation. The self-energy operator Σ describes exchange-correlation effects in the quasiparticle energies more successfully than the local, energy-independent exchange-correlation potential V_{xc} of the LDA. The difference between them is treated as a perturbation.

The central problem of this scheme is the calculation of the self-energy operator, which is performed in terms of the diagonal matrix elements in (7), $\langle\psi_{m\mathbf{k}}|\Sigma(E)|\psi_{m\mathbf{k}}\rangle$, using the wave functions from the LDA. As can be seen from (4), this requires an integral with respect to the energy ω. The dielectric matrices $\epsilon_{\mathbf{G},\mathbf{G}'}(\mathbf{q},\omega)$ have to be calculated and inverted for many values of ω. This is computationally very time consuming. Nevertheless, it has been carried out by some authors.[11] Instead, we use a plasmon-pole model[10,16,17] to describe approximately the dependence of $\epsilon^{-1}(\omega)$ on the frequency ω. In this scheme, only the calculation of the *static* dielectric matrices $\epsilon_{\mathbf{G},\mathbf{G}'}(\mathbf{q},\omega=0)$ is required. The quadrature with respect to ω is done analytically. In our approach, we use the method of the dielectric band structure[16–19] to introduce a plasmon-pole model. Considering that the static dielectric matrix $\epsilon_{\mathbf{G},\mathbf{G}'}(\mathbf{q},0)$ is Hermitian, its real eigenvalues $\lambda_{\mathbf{q}l}$ and orthonormal eigenvectors $\phi^l_{\mathbf{G}}$ can be used to perform the inversion of the matrix. The eigenvalues of the related full dielectric matrix are assumed to be dependent on the frequency, $\lambda_{\mathbf{q}l}(\omega)$, while the eigenvectors are independent of the frequency. This approximation, with a slightly different frequency dependence, has been discussed in detail by Hamada, Hwang, and Freeman.[20] For the inverse dielectric matrix, one obtains

$$\epsilon^{-1}_{\mathbf{G},\mathbf{G}'}(\mathbf{q},\omega)=\sum_l\phi^l_{\mathbf{G}}(\mathbf{q})\frac{1}{\lambda_{\mathbf{q}l}(\omega)}(\phi^l_{\mathbf{G}'}(\mathbf{q}))^* \ . \tag{8}$$

Within the plasmon-pole model, $\lambda_{\mathbf{q}l}(\omega)$ is assumed to be[16,17]

$$\lambda_{\mathbf{q}l}(\omega)=\left[1+\frac{z_{\mathbf{q}l}\omega_{\mathbf{q}l}}{2}\left[\frac{1}{\omega-(\omega_{\mathbf{q}l}-i0^+)}-\frac{1}{\omega+(\omega_{\mathbf{q}l}-i0^+)}\right]\right]^{-1} \ . \tag{9}$$

The parameters $z_{\mathbf{q}l}$ and $\omega_{\mathbf{q}l}$ are to be determined by adjusting (8) and (9) to the static dielectric matrix, and by taking Johnson's sum rule[21] into account. As a result, the diagonal matrix elements of the self-energy operator [cf. (7)] become

$$\langle\psi_{m\mathbf{k}}|\Sigma(E)|\psi_{m\mathbf{k}}\rangle$$
$$=\frac{4\pi e^2}{V}\sum_{\mathbf{q},\mathbf{G},\mathbf{G}'}\sum_{n}\frac{1}{|\mathbf{q}+\mathbf{G}|}\frac{1}{|\mathbf{q}+\mathbf{G}'|}\left[\int\psi^*_{m\mathbf{k}}(\mathbf{r})e^{-i(\mathbf{q}+\mathbf{G})\mathbf{r}}\psi_{n,\mathbf{k}+\mathbf{q}}(\mathbf{r})d^3r\right]\left[\int\psi^*_{m\mathbf{k}}(\mathbf{r})e^{-i(\mathbf{q}+\mathbf{G}')\mathbf{r}}\psi_{n,\mathbf{k}+\mathbf{q}}(\mathbf{r})d^3r\right]^*$$
$$\times\begin{cases}\displaystyle\sum_l\phi^l_{-\mathbf{G}}(-\mathbf{q})[\phi^l_{-\mathbf{G}'}(-\mathbf{q})]^*\left[-1+\frac{z_{-\mathbf{q}l}\omega_{-\mathbf{q}l}}{2}\frac{1}{E-E^{\mathrm{LDA}}_{n,\mathbf{k}+\mathbf{q}}+\omega_{-\mathbf{q}l}}\right] & \text{for } n\in VB\\ \displaystyle\sum_l\phi^l_{-\mathbf{G}}(-\mathbf{q})[\phi^l_{-\mathbf{G}'}(-\mathbf{q})]^*\left[\frac{z_{-\mathbf{q}l}\omega_{-\mathbf{q}l}}{2}\frac{1}{E-E^{\mathrm{LDA}}_{n,\mathbf{k}+\mathbf{q}}-\omega_{-\mathbf{q}l}}\right] & \text{for } n\in CB\ .\end{cases}\tag{10}$$

We have performed these full RPA calculations for all materials considered in this paper.

III. MODEL DIELECTRIC FUNCTIONS

Although some simplifications have been introduced, the method described above requires the time-consuming calculation of the static dielectric matrix $\epsilon_{\mathbf{G},\mathbf{G}'}(\mathbf{q},0)$ for some reciprocal vectors $\mathbf{q}$ from the first Brillouin zone. As can be seen from (10), the exact spatial behavior of the dielectric function is of minor importance. The sum $\Sigma_{\mathbf{q}\mathbf{G}\mathbf{G}'}$ means an averaging process, so that some general properties of the spatial behavior of the dielectric function should at last be sufficient to obtain reliable results for the band-structure energies. Concentrating on those properties, it should be possible to describe the dependence of $\epsilon_{\mathbf{G},\mathbf{G}'}(\mathbf{q},0)$ on $\mathbf{q}$ and on the reciprocal-lattice vectors $\mathbf{G},\mathbf{G}'$ by models. Usually, some specific properties of the material enter the models (e.g., electronic charge density, dielectric constant).

We have considered six different model dielectric matrices, starting from (a) the trivial model $\epsilon_{\mathbf{G},\mathbf{G}'}(\mathbf{q},0)=\delta_{\mathbf{G},\mathbf{G}'}$ of the Hartree-Fock theory, (b) the nondiagonal model of Hybertsen and Louie[22,23] that is based on a diagonal model by Levine and Louie,[24] and (c) a diagonal model suggested by Bechstedt, Enderlein, and Wischnewski.[25] The latter authors have extended their model to a nondiagonal one as well, but in our approach this extension is done in another way, as has been suggested by Falter.[26,27]

The model functions (b) and (c) require the value of the static dielectric constant as a central input. Since all ions are regarded as fixed within the Born-Oppenheimer approximation, this dielectric constant refers only to *electronic* effects. Therefore, the dielectric constant ϵ_∞ has to be used for ionic materials. Since there is no difference between ϵ_0 and ϵ_∞ for nonionic crystals, we label all dielectric constants ϵ_∞ throughout this paper for convenience. This refers to the static dielectric function of the electronic charge density only. We will now address various models in detail, separately.

(a) The most simple model is given by

$$\epsilon_{\mathbf{G},\mathbf{G}'}(\mathbf{q},0)=\delta_{\mathbf{G},\mathbf{G}'}\ .\tag{11}$$

Any spatial structure is neglected. Equation (10) becomes

$$\langle\psi_{m\mathbf{k}}|\Sigma(E)|\psi_{m\mathbf{k}}\rangle=-\frac{4\pi e^2}{V}\sum_{\mathbf{q},\mathbf{G}}\sum_{n\in VB}\frac{1}{|\mathbf{q}+\mathbf{G}|^2}\left|\int\psi^*_{m\mathbf{k}}(\mathbf{r})e^{-i(\mathbf{q}+\mathbf{G})\mathbf{r}}\psi_{n,\mathbf{k}+\mathbf{q}}(\mathbf{r})d^3r\right|^2\tag{12}$$
$$=-\sum_{\mathbf{q}'}\sum_{n\in VB}\int\psi^*_{m\mathbf{k}}(\mathbf{r})\psi^*_{n\mathbf{q}'}(\mathbf{r}')v(\mathbf{r},\mathbf{r}')\psi_{n\mathbf{q}'}(\mathbf{r})\psi_{m\mathbf{k}}(\mathbf{r}')d^3r\,d^3r'\ .\tag{13}$$

$v(\mathbf{r},\mathbf{r}')=e^2/|\mathbf{r}-\mathbf{r}'|$ means the pure Coulomb interaction. This result is equivalent to the expectation value of the Hartree-Fock exchange operator with respect to LDA wave functions.

(b1) Levine and Louie have developed a diagonal model.[24] Containing the explicit value of ϵ_∞, it takes into account the existence of a gap in the electronic structure of a semiconductor that does not occur in the homogeneous electron gas:

$$\epsilon_{\mathbf{G},\mathbf{G}'}(\mathbf{q},0)=\delta_{\mathbf{G},\mathbf{G}'}\epsilon_{\mathrm{LL}}(|\mathbf{q}+\mathbf{G}|,\bar\rho)\ ,\tag{14}$$
$$\epsilon_{\mathrm{LL}}(q,\bar\rho)=1+\frac{2}{\pi q_F}\left[\frac{1}{Q^2}-\frac{\lambda}{2Q^3}\left[\arctan\frac{2Q+Q^2}{\lambda}+\arctan\frac{2Q-Q^2}{\lambda}\right]+\left[\frac{\lambda^2}{8Q^5}+\frac{1}{2Q^3}-\frac{1}{8Q}\right]\ln\left[\frac{\lambda^2+(2Q+Q^2)^2}{\lambda^2+(2Q-Q^2)^2}\right]\right]\ .\tag{15}$$

Q has to be set to $Q=q/q_F$ and $\lambda=(\omega_{\mathrm{Pl}}/\omega_F)\sqrt{\epsilon_\infty-1}$, where ω_{Pl} is the plasma frequency, ω_F is the Fermi frequency, and q_F is the Fermi wave vector. These latter quantities all depend on the average electronic density $\bar\rho$.

(b2) The model of Levine and Louie has been extended into a nondiagonal one[22,23] that takes the inhomogeneity of the charge density much better into account. With

$$\epsilon^{-1}(\mathbf{r},\mathbf{r}')=\tfrac{1}{2}\epsilon^{-1}_{\mathrm{LL}}[|\mathbf{r}-\mathbf{r}'|,\rho(\mathbf{r})]+\tfrac{1}{2}\epsilon^{-1}_{\mathrm{LL}}[|\mathbf{r}-\mathbf{r}'|,\rho(\mathbf{r}')]\ ,\tag{16}$$

for the dielectric matrix one obtains:

$$\epsilon^{-1}_{\mathbf{G},\mathbf{G}'}(\mathbf{q},0)=\tfrac{1}{2}\int \epsilon^{-1}_{\mathrm{LL}}[|\mathbf{q}+\mathbf{G}|,\rho(\mathbf{r})]e^{-i(\mathbf{G}-\mathbf{G}')\cdot\mathbf{r}}d^3r + \tfrac{1}{2}\int \epsilon^{-1}_{\mathrm{LL}}[|\mathbf{q}+\mathbf{G}'|,\rho(\mathbf{r}')]e^{-i(\mathbf{G}-\mathbf{G}')\cdot\mathbf{r}'}d^3r' . \tag{17}$$

After calculating $\epsilon^{-1}_{\mathrm{LL}}[|\mathbf{q}+\mathbf{G}|,\rho(\mathbf{r})]$ on a special grid of $\mathbf{r}$ vectors, the Fourier transforms of Eq. (17) can be performed by fast-Fourier transform algorithms.

(c1) Another diagonal model has been suggested by Bechstedt, Enderlein, and Wischnewski:[25]

$$\epsilon(q,0)=1+\frac{\omega^2_{\mathrm{Pl}}}{\tilde{\omega}^2(q)} , \tag{18}$$

with

$$\tilde{\omega}^2(q)=\omega^2_{\mathrm{Pl}}\left[\frac{1}{\epsilon_\infty-1}+\left[\frac{q}{q_{\mathrm{TF}}}\right]^2\right]+\left[\frac{\hbar}{2m}\right]^2 q^4 , \tag{19}$$

where q_{TF} is the Thomas-Fermi wave vector.

(c2) According to Bechstedt, Enderlein, and Wischnewski, this diagonal model (18) and (19) can be extended into a nondiagonal model by[25]

$$\epsilon_{\mathbf{G},\mathbf{G}'}(\mathbf{q},0)=\delta_{\mathbf{G},\mathbf{G}'}+\frac{\omega^2_{\mathrm{Pl}}}{\tilde{\omega}^2[|\mathbf{q}+\frac{1}{2}(\mathbf{G}+\mathbf{G}')|]}\frac{(\mathbf{q}+\mathbf{G})}{|\mathbf{q}+\mathbf{G}|} \times\frac{(\mathbf{q}+\mathbf{G}')}{|\mathbf{q}+\mathbf{G}'|}\frac{\rho(\mathbf{G}-\mathbf{G}')}{\rho(\mathbf{0})} . \tag{20}$$

Unfortunately, this model yields dielectric matrices which have some eigenvalues that are smaller than 1 for some $\mathbf{q}$ vectors. Such matrices do not satisfy the requirements for thermodynamical stability of the solid.[19] They cannot be used for the plasmon-pole model of (8) and (9). Therefore, the diagonal model has to be extended in another way, e.g., by choosing the nondiagonal terms ($\mathbf{G}\neq\mathbf{G}'$), as has been suggested by Falter:[26,27]

$$\epsilon_{\mathbf{G},\mathbf{G}'}(\mathbf{q},0)=\delta_{\mathbf{G},\mathbf{G}'}+\frac{\omega^2_{\mathrm{Pl}}}{A(1+b|\mathbf{q}+\mathbf{G}|^2)(1+b|\mathbf{q}+\mathbf{G}'|^2)} \times\frac{(\mathbf{q}+\mathbf{G})}{|\mathbf{q}+\mathbf{G}|}\frac{(\mathbf{q}+\mathbf{G}')}{|\mathbf{q}+\mathbf{G}'|}\frac{\rho(\mathbf{G}-\mathbf{G}')}{\rho(\mathbf{0})} . \tag{21}$$

To make the new denominator $A(1+b|\mathbf{q}+\mathbf{G}|^2)(1+b|\mathbf{q}+\mathbf{G}'|^2)$ fit to the denominator $\tilde{\omega}^2(q)$ of the diagonal model (19), the parameter A has to be set to

$$A=\omega^2_{\mathrm{Pl}}\frac{1}{\epsilon_\infty-1} . \tag{22}$$

For further adjustment, we choose parameter b as

$$b=\frac{\hbar}{2m}\frac{\sqrt{\epsilon_\infty-1}}{\omega_{\mathrm{Pl}}} , \tag{23}$$

which agrees with the q^4 term of the denominator of the diagonal model (19). This model, which uses the diagonal model of Bechstedt, Enderlein, and Wischnewski (18) and (19) as its diagonal part, and the model suggested by Falter (21)–(23) as its nondiagonal part, is labeled (c2) from now on.

(c3) Alternatively, the model suggested by Falter can be used for both the nondiagonal *and* diagonal terms.[26] We have chosen parameters A and b as described above. This model, which uses Eqs. (21)–(23) for all $\mathbf{G},\mathbf{G}'$, is labeled (c3).

The nondiagonal models (b2), (c2), and (c3) require the inhomogeneous charge density that follows from the LDA calculations. All models require the value of the dielectric constant ϵ_∞ which is usually taken from experiment. This quantity can, as well, be *calculated* (see, e.g., Ref. 28) as

$$\epsilon_\infty=\left[\lim_{q\to 0}\epsilon^{-1}_{00}(\mathbf{q},0)\right]^{-1} . \tag{24}$$

This scheme requires the calculation of the dielectric matrix in RPA [cf. (6)] for one $\mathbf{q}$ point only. In this way, the dielectric constant need not be given as an empirical parameter.

IV. NUMERICAL DETAILS

A. Details of the LDA calculations

As can be seen from (7), the results of the LDA calculation enter into our *GW* scheme at several points. First, they enter into the approximation of the self-energy operator [see Eqs. (4)–(6)]. Second, the wave functions are used to calculate diagonal matrix elements of the self-energy operator. Third, the LDA band structure is used as the basis for the correction scheme given by the *GW* approximation. If model dielectric functions instead of the RPA matrices of (6) are used, the electronic density from the LDA enters into the scheme. Furthermore, the static electronic dielectric constant ϵ_∞ may be computed within the LDA, as described above. Inaccuracies within the LDA results will necessarily lead to inaccuracies of the *GW* approximation. Therefore, the LDA calculations must be carried out very carefully.

We use the nonlocal, norm-conserving *ab initio* pseudopotentials of Bachelet, Hamann, and Schlüter.[29] For diamond and SiC, the carbon ions are described by a similar pseudopotential constructed[30] by employing the procedure reported by Hamann, Schlüter, and Chiang.[31] Diamond and SiC are easier to calculate using this pseudopotential. For the exchange-correlation potential, we use the results of Ceperley and Alder,[32] as parametrized by Perdew and Zunger.[33]

Contrary to previous calculations by other authors, we use a basis set of localized functions (Gaussian orbitals) instead of plane waves. This leads to shorter computation time, especially if the material under consideration contains elements such as carbon that cause a strong localization of the wave functions. We have investigated different basis sets consisting of s, p, d, and s^* orbitals with up to 60 functions per unit cell. Our calculations show that already 40 Gaussians are sufficient to obtain band-structure energies that agree very well with the results of highly converged plane-wave calculations. Some details are given in Sec. V A.

To calculate the charge density from the wave func-

tions, ten special points[34] in the irreducible part of the Brillouin zone have been used.

B. Details of the *GW* calculations

All our *GW* calculations are carried out on the basis of the LDA calculations as described above. For the lattice constant a_0 and the dielectric constant ϵ_∞ (where necessary) the experimental values have been used.

One central problem within the realization of the *GW* approximation is the calculation of the spatial integrals that appear in (6) and (10). To achieve this, we write the Bloch functions, originally represented in terms of Gaussian orbitals, as a Fourier series

$$\psi_{m\mathbf{k}}(\mathbf{r})=\frac{1}{V}e^{i\mathbf{k}\cdot\mathbf{r}}\sum_{\mathbf{G}}C_{\mathbf{G}}^{m\mathbf{k}}e^{i\mathbf{G}\cdot\mathbf{r}}\ . \tag{25}$$

We note that in this case the coefficients $C_{\mathbf{G}}^{m\mathbf{k}}$ need not be determined by diagonalization of a respective Hamiltonian matrix, but simply follow from the known coefficients of the Gaussian basis. Resulting from (25), the integrals are evaluated as

$$\int\psi_{m\mathbf{k}}^*(\mathbf{r})e^{-i(\mathbf{q}+\mathbf{G})\cdot\mathbf{r}}\psi_{n,\mathbf{k}+\mathbf{q}}(\mathbf{r})d^3r = \frac{1}{V}\sum_{\mathbf{G}'}(C_{\mathbf{G}'}^{m\mathbf{k}})^*C_{\mathbf{G}+\mathbf{G}'}^{n,\mathbf{k}+\mathbf{q}}\ . \tag{26}$$

In our scheme, this sum takes account of a vector $\mathbf{G}'$ if both $|\mathbf{G}'|$ and $|\mathbf{G}+\mathbf{G}'|$ are smaller than a cutoff parameter. In general, up to 170 $\mathbf{G}'$ vectors are required for Si, Ge, and GaAs, and up to 260 $\mathbf{G}'$ vectors for diamond and SiC due to the stronger localization of the carbon wave functions. To apply this method to the special cases of $\mathbf{G}=\mathbf{0}$, $\mathbf{q}\approx\mathbf{0}$, and $m\neq n$, even more $\mathbf{G}'$ vectors are necessary in (26) to achieve sufficient accuracy. We use up to 1200 $\mathbf{G}'$ vectors for diamond.

All these integrals can in principle also be evaluated by utilizing the linear combination of Gaussian orbitals (LCGO) form of the basis functions. Instead of sums over reciprocal-lattice vectors, sums over neighboring atoms have to be performed. However, to reach the same degree of accuracy, this method takes more computation time.

The sum over $\mathbf{G}$ (and $\mathbf{G}'$) in (10) requires about 90 $\mathbf{G}$ vectors for Si, Ge, and GaAs, and up to 170 $\mathbf{G}$ vectors for diamond and SiC. The sum over $\mathbf{q}$ from the first Brillouin zone in (10) is performed by again using special points. Two special points and their stars give sufficient accuracy. The use of ten special points results in band-structure energy differences less than 0.05 eV (for Si).

If $\mathbf{G}=\mathbf{G}'=\mathbf{0}$ and $m=n$, the terms to be summed up in (10) diverge for small $\mathbf{q}$ such as $f(\mathbf{q})=A/q^2$. To perform the sum by special points, another function $g(\mathbf{q})$ has to be taken into account that shows the same behavior for $\mathbf{q}\to\mathbf{0}$: $g(\mathbf{q})\sim 1/q^2$. Now the summation can be done as follows:

$$\sum_{\mathbf{q}}f(\mathbf{q})\equiv\sum_{\mathbf{q}}[f(\mathbf{q})-Ag(\mathbf{q})]+A\sum_{\mathbf{q}}g(\mathbf{q})\ , \tag{27}$$

with

$$A=\lim_{q\to 0}[q^2f(\mathbf{q})]\ .$$

The term $f(\mathbf{q})-Ag(\mathbf{q})$ does not contain any divergency, so the first sum on the right-hand side of (27) can be evaluated by special points. The second sum on the right-hand side of (27), or the corresponding integral over the first Brillouin zone, is done analytically if $g(\mathbf{q})$ is chosen properly (see Ref. 35). If only one vector ($\mathbf{G}$ or $\mathbf{G}'$) is zero and $m=n$, the terms to be summed up in (10) behave like $f(\mathbf{q})=B/q$ for small $\mathbf{q}$. This problem is solved analogously, using another function that diverges like $1/q$ if $\mathbf{q}\to\mathbf{0}$. Since these divergencies are less problematic than the $1/q^2$ divergencies described above, we content ourselves with choosing $g(\mathbf{q})=1/q$ and calculating numerically its integral over the first Brillouin zone.

As can be seen from Eq. (10), the calculation of the self-energy matrix requires the computation of the dielectric matrix and the evaluation of (8) and (9) for each special point $\mathbf{q}$, and as well for $\mathbf{q}\to\mathbf{0}$ to determine quantities A and B in (27).

Usually, just inserting the LDA energy value $E_{m\mathbf{k}}^{\mathrm{LDA}}$ into the self-energy operator on the right-hand side of (7) is considered sufficient to obtain reliable band-structure values. This avoids further iterations of (7) with respect to the energy $E_{m\mathbf{k}}$. However, this procedure neglects the possibility that the matrix elements of the self-energy operator may depend on the energy E. Following Hybertsen and Louie, a somewhat better scheme is given by[10]

$$E_{m\mathbf{k}}\approx E_{m\mathbf{k}}^{\mathrm{LDA}}+\frac{\langle\psi_{m\mathbf{k}}|\Sigma(E_{m\mathbf{k}}^{\mathrm{LDA}})-V_{\mathrm{xc}}|\psi_{m\mathbf{k}}\rangle}{1-\left.\dfrac{\partial\langle\psi_{m\mathbf{k}}|\Sigma(E)|\psi_{m\mathbf{k}}\rangle}{\partial E}\right|_{E=E_{m\mathbf{k}}^{\mathrm{LDA}}}}\ . \tag{28}$$

The derivative $\partial\langle\psi_{m\mathbf{k}}|\Sigma(E)|\psi_{m\mathbf{k}}\rangle/\partial E$ in (28) is evaluated as a difference quotient. It is obtained without further expense. This scheme is used throughout our work.

When computing the dielectric matrices in RPA from (6), we evaluate the sum over $\mathbf{k}$ in (6) by the use of special points again. Two special points and their stars give sufficiently convergent results, except for the head of the dielectric matrix $\epsilon_{00}(\mathbf{q})$, which requires at least ten special points to reach a sufficient accuracy, especially for small $\mathbf{q}$ vectors.

V. RESULTS

First, we apply our approach to Si in order to investigate its accuracy and to scrutinize the applicability and use of the different model dielectric matrices in direct comparison. Thereafter, we investigate some other materials with diamond or zinc-blende structures: Ge, GaAs, diamond, and especially β-SiC (also known as 3C-SiC). All energy values refer to the valence-band maximum, that is set to 0 eV in each case.

A. Results for Si

For Si, we have carried out two sets of *GW* calculations, based on LDA calculations employing two different

basis sets. One of them uses 60 Gaussian orbitals (GO's) (decay constants: 0.18, 0.4, and 0.8 in atomic units). For the other one, 40 orbitals have been used (decay constants: 0.15 and 0.5). Starting from them, *GW* calculations have been performed including the full scheme which requires the calculation of the RPA matrices of Eq. (6). We have used the experimental lattice constant[36] $a_0 = 5.43$ Å.

The band-structure results at high-symmetry points are given in Table I. The LDA band structure and the full GWA band structure calculated with 40 GO's are shown in Fig. 1 in direct comparison.

First, we compare our LDA band-structure results to those of a highly converged plane-wave LDA calculation performed with 450 plane waves.[37] As can be seen from Table I, both our 60- and 40-GO LDA calculations yield nearly the same results as the 450-PW LDA calculation. This indicates that LDA calculations with localized functions are suitable to obtain reliable results for LDA band structures. Furthermore, our LDA calculations should be suitable to give a good foundation for the following *GW* computations. Second, we compare our *GW* results to the *GW* results of Hybertsen and Louie,[10] who used plane waves in their computation. The results of other authors[11,17] are not included in the table for direct comparison, because of slight differences between their approaches and our scheme. Godby, Schlüter, and Sham[11] did not use a plasmon-pole model. Hott[17] used empirical

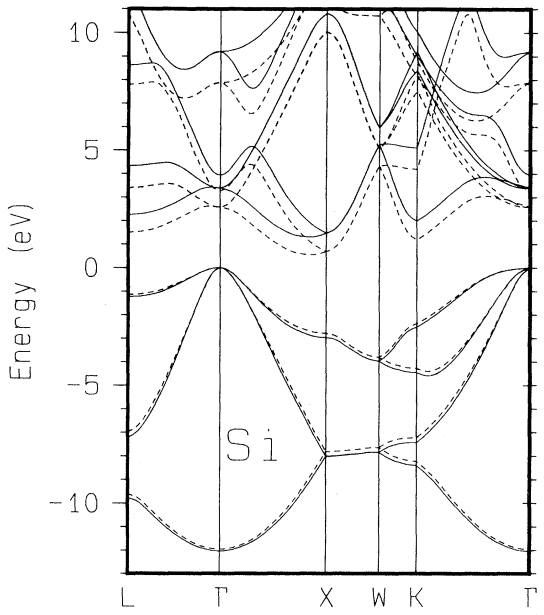

FIG. 1. Calculated electronic band structures along lines of high symmetry for Si (in eV). We show LDA and GWA results in comparison. The dashed lines display the LDA results calculated with 40 Gaussian orbitals (cf. Table I, column 2). The solid lines show the *GW* results based on these LDA calculations, using the full scheme with dielectric matrices in RPA (cf. Table I, column 5).

TABLE I. Calculated band-structure energies at points of high symmetry for Si (in eV). The LDA calculation of the third column has been performed by Chan, Vanderbilt, and Louie (Ref. 37), using plane waves. The *GW* calculations are performed using the full scheme of RPA matrices. The values of the sixth column have been calculated by Hybertsen and Louie (Ref. 10), using plane waves. The experimental data are from Ref. 36 except where noted otherwise.

Si	LDA 60 GO	LDA 40 GO	LDA[a] 450 PW	*GW* RPA 60 GO	*GW* RPA 40 GO	*GW*[b] RPA PW	Expt.[c]
Γ_{1v}	−11.91	−11.96	−11.91	−11.95	−12.04	−12.04	−12.5±0.6
Γ'_{25v}	0.00	0.00	0.00	0.00	0.00	0.00	0.0
Γ_{15c}	2.57	2.57	2.55	3.36	3.39	3.35	3.40,3.05[d]
Γ'_{2c}	3.24	3.28	3.28	3.89	3.93	4.08	4.23,4.1[d]
X_{1v}	−7.77	−7.81	−7.76	−7.95	−8.01		
X_{4v}	−2.78	−2.80	−2.86	−2.93	−2.98	−2.99	−2.9,[e] −3.3±0.2[f]
X_{1c}	0.65	0.68	0.66	1.43	1.47	1.44	1.25[d]
X_{4c}	10.03	10.04		10.76	10.80		
L'_{2v}	−9.58	−9.62	−9.56	−9.70	−9.77	−9.79	−9.3±0.4
L_{1v}	−6.94	−6.97	−6.96	−7.14	−7.21	−7.18	−6.7±0.2
L'_{3v}	−1.17	−1.14	−1.20	−1.25	−1.24	−1.27	−1.2±0.2, −1.5[g]
L_{1c}	1.47	1.51	1.50	2.19	2.26	2.27	2.1,[h] 2.4±0.15[i]
L_{3c}	3.32	3.40	3.33	4.25	4.33	4.24	4.15±0.1[i]
L'_{2c}	7.77	7.80		8.56	8.63		
E_{gap}	0.52	0.56		1.25	1.31	1.29	1.17

[a]Reference 37.
[b]Reference 10.
[c]Reference 36.
[d]Reference 38.
[e]Reference 39.
[f]Reference 40.
[g]Reference 41.
[h]Reference 42.
[i]Reference 43.

pseudopotentials instead of *ab initio* pseudopotentials. Our *GW* calculations, using 60 or 40 Gaussian orbitals, respectively, agree very well with the plane-wave *GW* results, as well. This shows that calculations using Gaussian orbitals are suited to obtain very good quasiparticle energies. Localized functions are as suitable as plane waves to perform state-of-the-art band-structure calculations. Minor differences in the numerical realization of the *GW* approximation, such as different plasmon-pole models or different treatments of divergencies [cf. (27)], seem to be of little importance.

Since our 60- and 40-GO results differ only very little, no more than 40 localized basis functions are necessary to perform convergent band-structure calculations (both within the LDA and within the GWA). For all materials investigated in this paper, we have carried out calculations with both 60 and 40 Gaussian orbitals, and found for most of the energies only very small differences in the LDA and GWA results, respectively. This holds if the decay constants are chosen carefully.

On comparing the GWA results to the LDA, the valence-band energies are shifted to lower energies by a small amount. On the contrary, the conduction-band states rise in energy. They are shifted to higher energies nearly rigidly. As can be seen from Table I, our GWA band-structure results are in good agreement with experimental data. In particular, the gap problem no longer occurs. We come back to a more detailed comparison with experimental data further below in the discussion of Fig. 3.

In addition to the calculations based on the RPA, we have performed analogous *GW* calculations using the model dielectric functions as described in Sec. III. The experimental value of the dielectric constant[36] $\epsilon_\infty = 11.7$ has been used. In Table II we compare the band-structure energies resulting for the six different models with one another. For direct comparison the full RPA-GWA results from column 5 of Table I are given, as well.

TABLE III. Calculated band-structure energies at points of high symmetry for Si (in eV), based on the 40 GO LDA calculation that is shown in Table I, column 2. The full *GW* calculation using dielectric matrices in RA has been performed here. The results of the first column have been obtained by just inserting the LDA energies into the self-energy operator in (7). The results of the second column have been calculated by using Eq. (28). The latter scheme is used throughout our work (therefore, this column is the same as column 5 of Table I).

Si	Simple scheme	Scheme of (28)
Γ_{1v}	−12.14	−12.04
Γ'_{25v}	0.00	0.00
Γ_{15c}	3.63	3.39
Γ'_{2c}	4.11	3.93
X_{1v}	−8.11	−8.01
X_{4v}	−3.02	−2.98
X_{1c}	1.67	1.47
X_{4c}	11.05	10.80
L'_{2v}	−9.88	−9.77
L_{1v}	−7.31	−7.21
L'_{3v}	−1.27	−1.24
L_{1c}	2.45	2.26
L_{3c}	4.59	4.33
L'_{2c}	8.87	8.63
E_{gap}	1.50	1.31

TABLE II. Calculated band-structure energies at points of high symmetry for Si (in eV), based on the 40 GO LDA calculation that is shown in Table I, column 2. The *GW* calculations have been performed using the model dielectric functions that are described in the text (see Sec. III). These results should be compared to the corresponding full *GW* calculation. Therefore, the results of this full calculation (column 5 in Table I) are listed again in this table (last column) for the convenience of the reader.

Si	(a) 40 GO	(b1) 40 GO	(b2) 40 GO	(c1) 40 GO	(c2) 40 GO	(c3) 40 GO	RPA 40 GO
Γ_{1v}	−17.29	−12.46	−12.45	−12.44	−12.37	−12.04	−12.04
Γ'_{25v}	0.00	0.00	0.00	0.00	0.00	0.00	0.00
Γ_{15c}	8.56	3.17	3.20	3.14	3.33	3.17	3.39
Γ'_{2c}	10.01	3.97	3.88	3.97	4.00	3.82	3.93
X_{1v}	−11.28	−8.26	−8.22	−8.22	−8.20	−8.03	−8.01
X_{4v}	−3.92	−3.09	−3.05	−3.05	−3.03	−2.99	−2.98
X_{1c}	6.38	1.07	1.21	1.05	1.33	1.16	1.47
X_{4c}	18.67	10.88	10.48	10.86	10.99	10.69	10.80
L'_{2v}	−13.96	−10.10	−10.07	−10.07	−10.04	−9.78	−9.77
L_{1v}	−9.93	−7.43	−7.37	−7.37	−7.35	−7.22	−7.21
L'_{3v}	−1.61	−1.28	−1.27	−1.27	−1.27	−1.24	−1.24
L_{1c}	7.43	2.05	2.08	2.03	2.19	2.04	2.26
L_{3c}	9.78	4.05	4.12	4.01	4.25	4.07	4.33

All these calculations were done using the 40-GO basis.

The dielectric models result in similar behavior of the band-structure energies to that found for the RPA matrix of the full calculation scheme. The valence bands shift to lower while the conduction bands shift to higher energies. As one would expect, the results of the nondiagonal models agree better with those of the full calculation than do those of the diagonal models. The Hartree-Fock results (a) do not give any reasonable description of the material. The valence bands are lowered and the conduction bands are raised too much. Obviously, our results reflect the well-known fact that Hartree-Fock theory is not appropriate for the description of the electronic properties of a semiconductor.[17,35] Model (b2), which was developed by Hybertsen and Louie, agrees well with the results of the full calculation. It gives a good approximation of all band-structure energies, but still underestimates the fundamental gap. Model (c2), which contains the model of Bechstedt, Enderlein, and Wischnewski as its diagonal terms, and the model suggested by Falter as its nondiagonal ones, approximate the band-structure energies of the full *GW* calculation well, especially near the fundamental gap (from about -3 to $+5$ eV). Nevertheless, it yields a smaller gap than the full calculation. Model (c3), which uses the analytical form suggested by Falter for all terms, reproduces the valence-band energies of the full calculation in an excellent way, including the low ones.

As mentioned above, inserting the LDA band-structure energies into the self-energy operator in (7) is often considered to give satisfying results. If the improved scheme of Hybertsen and Louie, taking the dynamical properties of $\Sigma(E)$ better into account, is used [see Eq. (28)], the results change noticeably. This is shown in Table III, where the results of both approaches are compared for the full calculation, using the RPA matrix and 40 GO's. Compared to the simple scheme, the scheme of (28) makes the valence-band energies rise slightly, while the conduction-band energies drop a bit. This behavior agrees with the fact that the matrix elements of the self-energy operator, $\langle \psi_{m\mathbf{k}} | \Sigma(E) | \psi_{m\mathbf{k}} \rangle$, have a negative slope with respect to the energy E, as can be expected from the theory of the Green's function,[44] and as has already been discussed by Hybertsen and Louie.[10]

Finally, in the case of Si we investigated the dependence of the results on the value of the dielectric constant ϵ_∞, which enters as a parameter for models (b) and (c). For this purpose, we have chosen model (c2) and performed *GW* calculations using different values of ϵ_∞ (11.0, 12.0, and 13.0), chosen *ad hoc*. The respective band-structure energies are given in Table IV.

If ϵ_∞ changes from 11.0 to 13.0 the absolute values of the band-structure energies become smaller, but change by less than 0.1 eV. This shows that the results do not depend crucially on the value of ϵ_∞. An approximate value of the dielectric constant ϵ_∞ is thus sufficient to perform *GW* calculations using a model dielectric function. We come back to this aspect in Sec. VI.

TABLE IV. Calculated band-structure energies at points of high symmetry for Si (in eV). The energies have been calculated using the model dielectric function (c2). Several values of the dielectric constant ϵ_∞ have been investigated, showing the dependence of the band-structure results on it.

ϵ_∞	11.0	12.0	13.0
Γ_{1v}	−12.38	−12.35	−12.33
Γ'_{25v}	0.00	0.00	0.00
Γ_{15c}	3.36	3.33	3.31
Γ'_{2c}	4.03	4.00	3.97
X_{1v}	−8.22	−8.20	−8.18
X_{4v}	−3.03	−3.03	−3.02
X_{1c}	1.35	1.32	1.31
X_{4c}	11.02	10.98	10.95
L'_{2v}	−10.04	−10.03	−10.00
L_{1v}	−7.36	−7.35	−7.32
L'_{3v}	−1.27	−1.27	−1.25
L_{1c}	2.22	2.19	2.18
L_{3c}	4.29	4.25	4.23
L'_{2c}	8.52	8.48	8.45
E_{gap}	1.20	1.17	1.16

B. Results for Ge, GaAs, and diamond

We have carried out similar calculations for Ge, GaAs, and diamond. The results are based on LDA calculations with 40 Gaussian orbitals (Tables VI–VIII). The 40-GO LDA band structures and the respective full *GW* band structures are compiled in Fig. 2. The lattice constants, dielectric constants, and decay constants of the wave functions are given in Table V.

We remind the reader that the dielectric constant ϵ_∞ rather than ϵ_0 must be used for ionic crystals, to take account of the electronic part of the dielectric function only.

For all three materials, in Tables VI–VIII we give the LDA band-structure energies as well as the results of the full *GW* calculations. Furthermore, results obtained with model (c2) for the dielectric matrix are shown. We have chosen this model since for Si it yields a good overall agreement with the results of our full *GW* calculation, as we have seen in Table II. All results are compared to experimental data as well. We have also performed calculations with 60 basis functions. The differences in the band

TABLE V. Lattice constants (in Å), dielectric constants, and decay parameters, as used for our calculations. The lattice constants and the dielectric constants are from Ref. 36.

	a_0[a]	ϵ_∞[a]	Decay parameters
Si	5.43	11.7	0.15,0.5
Ge	5.66	16.0	0.2,0.5
GaAs	5.65	10.9	0.2,0.5 for Ga, 0.2,0.5 for As
C	3.57	5.7	0.35,1.4
SiC	4.36	6.5	0.2,0.5 for Si, 0.35,1.4 for C

[a]Reference 36.

structures from the results displayed here are small. As was found for Si, 40-GO basis functions are sufficient to give reliable results. Similar to the case of Si, the valence bands are shifted to lower energies by a small amount. For diamond, the first valence band is lowered by more than 1 eV. The conduction-band energies of all materials rise considerably, and agree well with experimental results. In comparison to the full calculations, the model calculations show the same behavior as that found for Si. Model functions (b2) and especially (c2) yield good results in the gap region, while model function (c3) reproduces the valence-band energies of the full calculation very well.

Our results for Ge are given in Table VI. The LDA yields a fundamental gap which nearly vanishes. In GWA the gap is enormously improved, but remains direct instead of indirect. We compare the results of our full *GW* calculation to those of Hybertsen and Louie.[10] Our band-structure results show very good agreement with those values and with the experimental data except for a few states, most noticeably $E(L'_{2c})$. With 60 Gaussian orbitals we obtain 7.46 eV in LDA and 8.11 eV in GWA for $E(L'_{2c})$. The results of Hybertsen and Louie show a direct gap as well. It should be noted that taking account of core polarization results in even better band-structure energies. In particular, the fundamental gap of Ge becomes indirect.[45]

The band-structure energies for GaAs are listed in Table VII. The general improvement of the results of the *GW* approximation is similar to that found for Si or Ge, and leads to a reliable electronic band structure, although some values do not match experiment perfectly. Also in

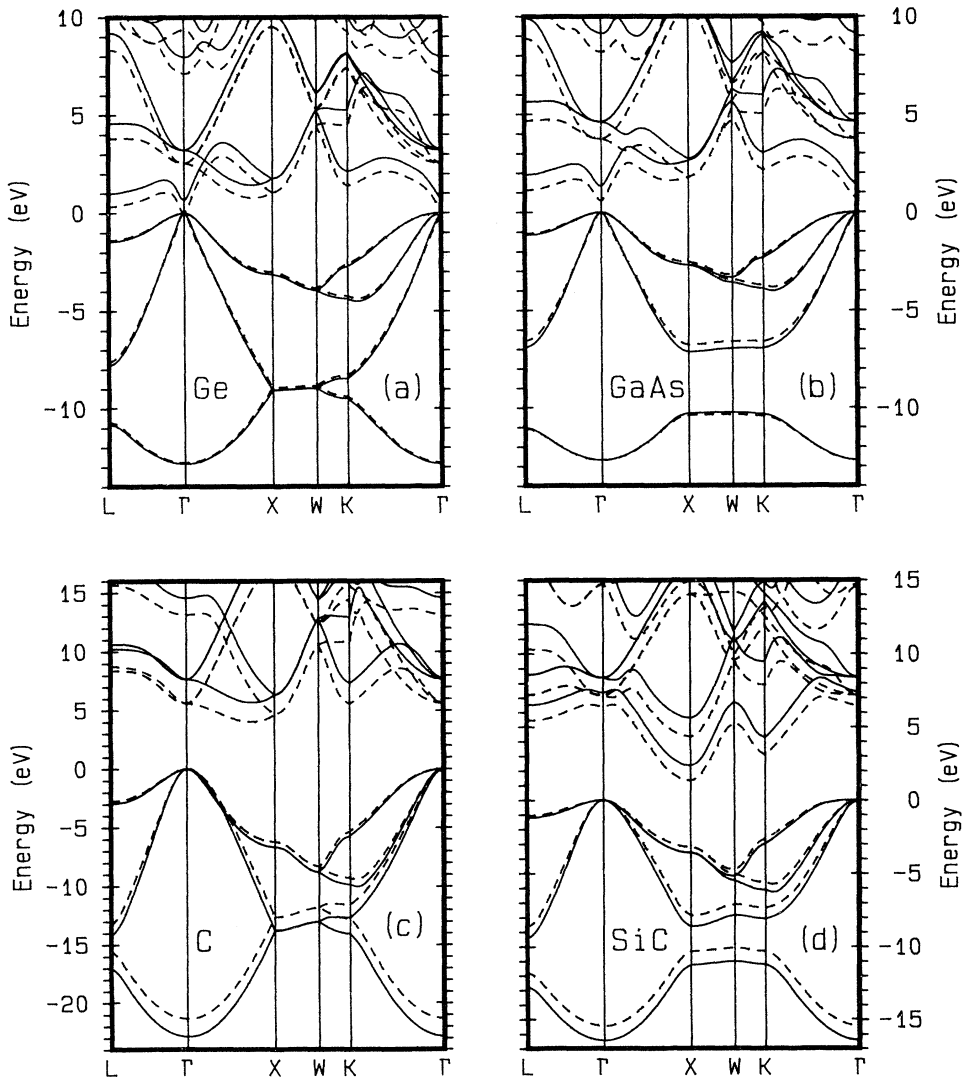

FIG. 2. Calculated electronic band structures along lines of high symmetry for (a) Ge, (b) GaAs, (c) diamond, and (d) β-SiC (in eV). We show LDA and GWA results in comparison. The dashed lines display the LDA results calculated with 40 Gaussian orbitals (cf. column 1 of Tables VI–IX for Ge, GaAs, diamond, and SiC, respectively). The solid lines show the GWA results based on these LDA calculations, using the full scheme with dielectric matrices in RPA (cf. column 2 of Tables VI–IX for Ge, GaAs, diamond, and SiC, respectively).

TABLE VI. Calculated band-structure energies at points of high symmetry for Ge (in eV). The *GW* calculations have been performed using both the full scheme of dielectric matrices in RPA (column 2) and the model dielectric function (c2), which is described in Sec. III (column 3). The results of column 4 have been obtained by Hybertsen and Louie (Ref. 10) who have performed a full *GW* calculation using plane waves. It should be noted that effects of spin-orbit coupling have been included in this calculation. The experimental data are from Ref. 36 except where noted otherwise.

Ge	LDA 40 GO	GWA (RPA) 40 GO	GWA (c2) 40 GO	GWA[a] (RPA) PW	Expt.[b]
Γ_{1v}	−12.79	−12.84	−12.99	−12.86	−12.6, −12.9±0.2[c]
Γ'_{25v}	0.00	0.00	0.00	0.00, −0.30	0.0
Γ'_{2c}	0.01	0.65	0.57	0.71	0.89[d]
Γ_{15c}	2.53	3.21	3.12	3.04,3.26	3.01,[d]3.21[d]
X_{1v}	−8.91	−9.06	−9.17	−9.13	−9.3±0.2[c]
X_{4v}	−3.02	−3.16	−3.18	−3.22	−3.15±0.2, −3.5±0.2[c]
X_{1c}	1.03	1.74	1.59	1.23	1.3±0.2
X_{3c}	9.54	10.19	10.25		
L'_{2v}	−10.71	−10.82	−10.94	−10.89	−10.6±0.5
L_{1v}	−7.63	−7.81	−7.90	−7.82	−7.7±0.2
L'_{3v}	−1.40	−1.47	−1.48	−1.61, −1.43	−1.4±0.3
L_{1c}	0.33	0.98	0.86	0.75	0.744
L_{3c}	3.80	4.57	4.48	4.33,4.43	4.3±0.2,4.2±0.1[e]
L'_{2c}	8.33	9.20	9.03	7.61	7.8±0.6,7.9±0.1[e]
E_{gap}	0.01	0.65	0.57	0.71	0.744

[a]Reference 10.
[b]Reference 36.
[c]Reference 40.
[d]Reference 46.
[e]Reference 47.

this case we find an appreciable deviation for $E(L_{1c})$, which is similar to the deviation mentioned above for Ge. In this case we obtain with 60 Gaussian orbitals 8.08 eV in LDA and 8.86 eV in GWA for $E(L_{1c})$. We do not display the results of other authors for GaAs, because of some differences in their approaches[11,17] to our scheme.

Our results for diamond are given in Table VIII, in comparison with those of Ref. 10 and with available experimental data. The agreement with experiment is not perfect, as also has been found by Hybertsen and Louie.[10] But neither is it bad, and the calculated gap energy compares extremely well with the data.

In Fig. 2 we have compiled all the results from our LDA and GWA calculations using the full RPA matrices and the 40-GO basis sets. In addition to Ge, GaAs, and diamond, we have included our results for SiC, which will be discussed in detail in Sec. V C. This compilation highlights similarities and differences between the band structures of these four important materials.

To allow a direct comparison with experiment of our GWA results for Si, Ge, and GaAs, as calculated with 40-GO basis sets using the full RPA dielectric matrices, in Fig. 3 we show the respective band structures along the L-Γ-X high-symmetry lines, together with available experimental data from photoemission and inverse photoemission spectroscopy. A similar comparison has been given recently by Ortega and Himpsel[38] in their paper on inverse photoemission spectroscopy results for these three solids. While these authors had to compare their data to theoretical results from two different sources,[10,23] here we compare a full body of experimental data to

TABLE VII. Calculated band-structure energies at points of high symmetry for GaAs (in eV). The *GW* calculations have been performed using both the full scheme of dielectric matrices in RPA (column 2) and the model dielectric function (c2), which is described in Sec. III (column 3). The experimental values are from Ref. 36 except where noted otherwise.

GaAs	LDA	GWA (RPA)	GWA (c2)	Expt.[a]
Γ_{1v}	−12.69	−12.69	−12.91	−13.21
Γ_{15v}	0.00	0.00	0.00	0.0
Γ_{1c}	0.57	1.32	1.25	1.52
Γ_{15c}	3.73	4.60	4.54	4.61
X_{1v}	−10.37	−10.27	−10.53	−10.86
X_{3v}	−6.79	−7.16	−7.17	−6.81
X_{5v}	−2.56	−2.71	−2.73	−2.91
X_{1c}	1.80	2.65	2.53	1.90
X_{3c}	1.85	2.72	2.60	2.47
X_{5c}	10.33	11.20	11.27	
L_{1v}	−11.08	−11.02	−11.27	−11.35
L_{1v}	−6.59	−6.91	−6.94	−6.81
L_{3v}	−1.10	−1.17	−1.20	−1.41
L_{1c}	1.13	1.92	1.84	1.74
L_{3c}	4.67	5.65	5.56	5.45[b]
L_{1c}	8.88	9.92	9.78	8.6[b]
E_{gap}	0.57	1.32	1.25	1.52

[a]Reference 36.
[b]Reference 38.

theoretical results obtained on equal footing from one single approach. We observe a very good overall agreement between theory and experiment. In the case of Ge, the agreement is excellent except for the highest measured band on the Λ line from Γ to L. For GaAs the agreement is very good, and again we find pronounced deviations only for the highest conduction band measured. The plane-wave results in Ref. 10 for Ge and in Ref. 23 for GaAs agreed very well with this measured band, as well (see Fig. 6 of Ref. 38 for that matter). We had mentioned these particular differences already in discussion of Tables VI and VII. This single deviation high up in the conduction bands seems to be the only price one has to pay for the computational advantages of using a 40-Gaussian-orbital basis set. If a 60-Gaussian-orbital basis set is used, the agreement between theory and experiment is very good for these states, as well. In the case of Si, our results reproduce the experimental data very well. The same type of agreement was observed for the results of Zhu and Louie[23] (see again Fig. 6 of Ref. 38). In summary, Fig. 3 highlights the type of agreement one obtains nowadays between experiment and state-of-the-art electronic structure calculations for the three most important semiconductor materials Si, Ge, and GaAs, when the *GW* approximation together with the full RPA dielectric matrix is employed.

TABLE VIII. Calculated band-structure energies at points of high symmetry for diamond (in eV). The *GW* calculations have been performed using both the full scheme of dielectric matrices in RPA (column 2) and the model dielectric function (c2), which is described in Sec. III (column 3). The results of column 4 have been obtained by Hybertsen and Louie (Ref. 10), who have performed a full *GW* calculation using plane waves. The experimental data are from Ref. 36 except where noted otherwise.

C	LDA 40 GO	GWA (RPA) 40 GO	GWA (c2) 40 GO	GWA[a] (RPA) PW	Expt.[b]
Γ_{1v}	−21.35	−22.88	−23.42	−23.0	−24.2±1, −21±1
Γ'_{25v}	0.00	0.00	0.00	0.0	0.0
Γ_{15c}	5.58	7.63	7.54	7.5	7.3
Γ'_{2c}	13.10	14.54	14.68	14.8	15.3±0.5[c]
X_{1v}	−12.61	−13.80	−14.15		
X_{4v}	−6.26	−6.69	−6.86		
X_{1c}	4.63	6.30	6.04		
X_{4c}	16.91	19.50	19.92		
L'_{2v}	−15.51	−16.95	−17.39	−17.3	−15.2±0.3[c]
L_{1v}	−13.33	−14.27	−14.61	−14.4	−12.8±0.3[c]
L'_{3v}	−2.78	−2.98	−3.05		
L_{1c}	8.39	10.63	10.56		
L_{3c}	8.76	10.23	10.16		
L'_{2c}	15.67	18.14	18.15	17.9	20±1.5[c]
E_{gap}	4.01	5.67	5.43	5.6	5.48

[a]Reference 10.
[b]Reference 36.
[c]Reference 48.

C. Results for β-SiC

As a last material, we investigated cubic SiC. The band-structure results are displayed in Table IX. Since our results are the first quasiparticle energies for SiC, we summarize the band-structure results of several of our *GW* calculations, using both the full RPA matrix as well as the three nondiagonal models for the dielectric matrix that have been described above [(b2), (c2), and (c3)]. They are based again on a 40-GO LDA calculation (for the decay parameters, see Table V). The experimental values of the lattice constant and of the dielectric constant ϵ_∞ (for the models) have been used (cf. Table V).

A few band-structure energies have been measured so far. Our GWA results of the full calculation agree amazingly well with the data, except for $E(L_{1c})$ and $E(\Gamma_{15c})$. $E(L_{1c})$ is overestimated even by the LDA, which is very strange. Many of those experimental data have been obtained by reflectivity measurements. The classification of measured values as belonging to a certain point in the Brillouin zone may yet not be definite. Further measurements, in particular by photoemission and inverse photoemission spectroscopy, may give more detailed information on the band structure. The fundamental gap is given excellently by our calculation.

The model dielectric functions exhibit the same behavior in these results as they do for Si. Model (b2) largely agrees with the full calculation except for the lowest valence band. Model (c2) gives good energies around the gap region, while model (c3) reproduces the valence-band energies of the full calculation excellently.

TABLE IX. Calculated band-structure energies at points of high symmetry for β-SiC (in eV). The *GW* calculations have been performed using both the full scheme of dielectric matrices in RPA (column 2) and the model dielectric functions (b2), (c2), and (c3), which are described in Sec. III (columns 3–5). The experimental results are taken from Ref. 36.

SiC	LDA	GWA (RPA)	GWA (b2)	GWA (c2)	GWA (c3)	Expt.[a]
Γ_{1v}	−15.44	−16.44	−17.05	−16.75	−16.54	
Γ_{15v}	0.00	0.00	0.00	0.00	0.00	0.0
Γ_{1c}	6.41	7.35	7.35	7.42	7.24	
Γ_{15c}	7.16	8.35	8.29	8.54	8.35	7.75
X_{1v}	−10.31	−11.24	−11.77	−11.56	−11.46	
X_{3v}	−7.89	−8.64	−8.75	−8.71	−8.65	
X_{5v}	−3.22	−3.62	−3.69	−3.66	−3.65	−3.6
X_{1c}	1.31	2.34	2.14	2.35	2.18	2.39
X_{3c}	4.33	5.59	5.42	5.66	5.48	5.5,4.7
X_{5c}	14.05	15.78	15.99	16.15	15.91	
L_{1v}	−11.80	−12.75	−13.29	−13.06	−12.93	
L_{1v}	−8.63	−9.42	−9.55	−9.48	−9.43	
L_{3v}	−1.06	−1.21	−1.24	−1.22	−1.22	−1.16
L_{1c}	5.46	6.53	6.46	6.64	6.46	4.2
L_{3c}	7.20	8.57	8.45	8.71	8.52	8.5
L_{1c}	10.31	12.04	12.08	12.19	11.97	
E_{gap}	1.31	2.34	2.14	2.35	2.18	2.39

[a]Reference 36.

In general, they give an overall description of the band structure of cubic SiC which is as reliable as that of the full calculation.

VI. THE DIELECTRIC CONSTANT ϵ_∞

In this section we will discuss our results for the dielectric constant ϵ_∞ which we have calculated from Eqs. (6) and (24). The wave vector $\mathbf{q}$ has been chosen along the (1,0,0) direction ($\mathbf{q}\|\mathbf{q}_x, \mathbf{q}\to\mathbf{0}$). We have done this evaluation for both our 60- and 40-GO LDA calculations. The results are displayed in Table X. For ionic crystals this method yields only the electronic part of the dielectric constant, ϵ_∞.

Since our 60- and 40-GO results agree rather well, the use of 40 bands seems to be sufficient to compute the dielectric constants as well. We compare our results to those of other authors[28,52] and find good overall agreement. Nevertheless, the agreement is not perfect. This may result from the fact that we have used no more than ten special points in the calculation of $\epsilon_{GG'}(\mathbf{q},0)$.

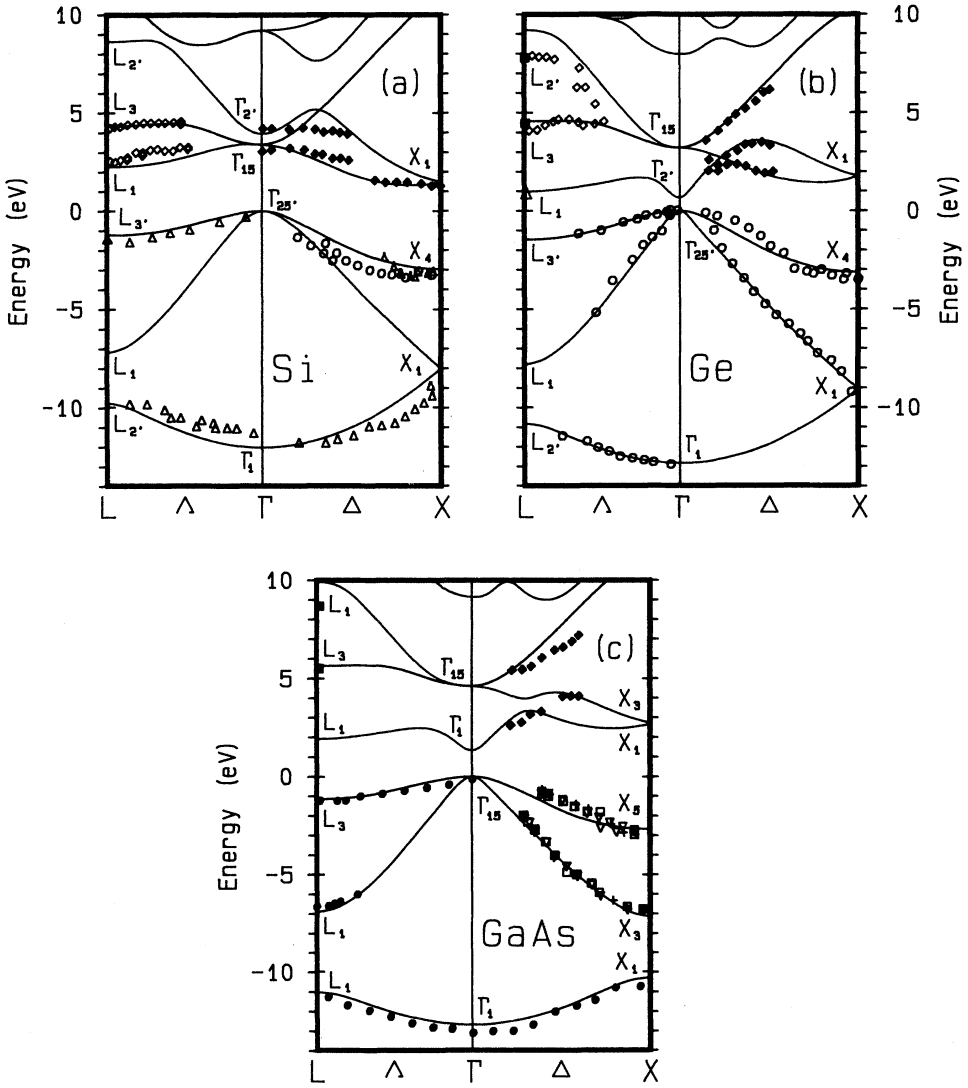

FIG. 3. Calculated electronic band structures along lines of high symmetry for (a) Si, (b) Ge, and (c) GaAs (in eV). We show GWA results and experimental data in comparison. The solid lines show the 40 GO GWA results, using the full scheme with dielectric matrices in RPA (cf. Table I, column 5 for Si; Table VI, column 2 for Ge; and Table VII, column 2 for GaAs). The experimental data have been obtained by photoemission and inverse photoemission. They were summarized in a recent paper on inverse photoemission spectroscopy by Ortega and Himpsel (cf. Fig. 6 of Ref. 38). The symbols refer to different works: full diamonds and full squares, from Si(100)-(2×1), Ge(100)-(2×1), and GaAs(100)-(4×2) surfaces (Ref. 38); open circles, from Si(100)-(2×1), Ge(111)-c(2×8), Ge(111)-(1×1)H, and Ge(100) (Ref. 40); full triangle, from Si(111)-(2×1) (Ref. 41); open diamonds, from Si(111)-(2×1) and Ge(111)-(2×1) (Ref. 47); open triangles, from Sb-saturated Si(100) and Si(111) (Ref. 49); open squares, open dels, and crosses, from GaAs(100)-(1×1), GaAs(100)-c(2×8), and GaAs(100)-c(6×4), respectively (Ref. 50); filled circles, from GaAs(110) (off-normal) (Ref. 51).

TABLE X. Calculated dielectric constants, obtained from our 60 GO LDA calculations and from our 40 GO LDA calculations for $\mathbf{q}\|(1,0,0), \mathbf{q}\to\mathbf{0}$. The values of the third column have been computed by Hybertsen and Louie (Ref. 28), and by Baroni and Resta (Ref. 52) using plane waves. The experimental data are from Ref. 36.

	ϵ_∞ 60 GO	ϵ_∞ 40 GO	ϵ_∞ PW[a]	ϵ_∞ Expt.[b]
Si	12.8	12.7	12.2, 12.04[c]	11.7
Ge	21.8	20.3	19.2	16.0
GaAs	13.1	12.2		10.9
C	5.5	5.5	5.62	5.7
SiC	6.7	6.6		6.5

[a]Reference 28, except where noted.
[b]Reference 36.
[c]Reference 52.

The calculated dielectric constants of GaAs and especially of Ge are somewhat larger than the experimental values. This may result from the fact that the LDA underestimates the fundamental gap, especially for Ge. The energy differences between occupied and unoccupied states enter into the dielectric matrices in terms of a denominator [cf. (6)]. Therefore, underestimation of the fundamental gap leads directly to an overestimation of the dielectric constant.

The dependence of band-structure energies, however, on the value of the dielectric constant was not very strong for Si (see Table IV). In order to investigate the influence of the dielectric constant on the band-structure results of other materials, as well, it is interesting to perform *GW* calculations with a model dielectric function using our *calculated* dielectric constants. For this matter, we have chosen the model dielectric function (c2). For the calculated dielectric constants, we have taken the results from our 40-GO LDA calculations (cf. column 2 in Table X). The band-structure results are compared to those obtained when using the *experimental* values of the dielectric constants for the same model. To represent the main properties of the band structures, we concentrate on the results for the fundamental gap, $E_{\rm gap}$, and the valence-band width W. The results are displayed in Table XI.

A larger dielectric constant in general results in a slightly lower fundamental gap, as is found for all materials considered here. Nevertheless, this influence is not very strong, even for Ge, where our calculated dielectric constant ϵ_∞ is overestimated by as much as 20%. The valence-band width is hardly affected by the value of the dielectric constant.

TABLE XI. Dependence of the calculated electronic gap $E_{\rm gap}$ and the calculated valence-band width W (in eV) on the value of the dielectric constant, which is used as an input parameter for the model dielectric functions. We compare the experimental dielectric constants (column 1; from Ref. 36) to the corresponding calculated values (column 4) that have been obtained from our 40 GO LDA calculations (cf. Table X, column 2). The band-structure values are calculated using the model dielectric function (c2), that has been introduced in Sec. III. The results obtained with the experimental values of the dielectric constants (columns 2 and 3) are compared to those obtained with the calculated dielectric constants (columns 5 and 6).

	ϵ_∞ (Expt.[a])	$E_{\rm gap}$ *GW*(c2)	W *GW*(c2)	ϵ_∞ (calc.)	$E_{\rm gap}$ *GW*(c2)	W *GW*(c2)
Si	11.7	1.17	12.37	12.7	1.16	12.34
Ge	16.0	0.57	12.99	20.3	0.50	12.97
GaAs	10.9	1.25	12.91	12.2	1.21	12.88
C	5.7	5.43	23.42	5.5	5.47	23.46
SiC	6.5	2.35	16.75	6.6	2.33	16.74

[a]Reference 36.

VII. SUMMARY

In this paper we have presented calculations of quasiparticle band structures for semiconductors and insulators. The required self-energy operator is evaluated within the *GW* approximation. It yields energy corrections to carefully performed LDA calculations. We have used basis sets of Gaussian orbitals. Norm-conserving *ab initio* pseudopotentials have been employed to obtain very good wave functions from the LDA. For the dielectric matrix, both the full RPA expression and several model functions have been employed. The nondiagonal model functions yield band-structure results in good agreement with the results of the full *GW* calculations using the dielectric matrix in RPA.

We have presented calculations for Si, Ge, GaAs, diamond, and β-SiC. Our results are in very good agreement with experimental data. Our scheme, based on relatively small basis sets of localized Gaussian orbitals, turns out to be a powerful method for the calculation of quasiparticle energies and excitation spectra of semiconductors and insulators. It should be applicable to more complex systems such as bulk defects, surfaces, and interfaces.

ACKNOWLEDGMENTS

It is our great pleasure to thank C. Falter for bringing his work on model dielectric functions to our attention. Furthermore we would like to acknowledge fruitful discussions with F. Bechstedt, C. Falter, and M. Sabisch.

[1]P. Hohenberg and W. Kohn, Phys. Rev. **136**, B864 (1964).
[2]W. Kohn and L. J. Sham, Phys. Rev. **140**, A1133 (1965).
[3]*Theory of the Inhomogeneous Electron Gas,* edited by S. Lundqvist and N. H. March (Plenum, New York, 1983), and references therein.
[4]*Electronic Structure, Dynamics, and Quantum Structural Properties of Condensed Matter,* edited by J. T. Devreese and P. Van Camp, Vol. 121 of *NATO Advanced Study Institute, Series B: Physics* (Plenum, New York, 1985), and references therein.

[5]W. E. Pickett, Comm. Solid State Phys. **12**, 1 (1985).
[6]G. B. Bachelet and N. E. Christensen, Phys. Rev. B **31**, 879 (1985).
[7]P. Schröer, P. Krüger, and J. Pollmann, Phys. Rev. B **47**, 6971 (1993).
[8]L. Hedin, Phys. Rev. **139**, A796 (1965).
[9]L. Hedin and S. Lundqvist, in *Solid State Physics, Advances in Research and Application,* edited by F. Seitz, D. Turnbull, and H. Ehrenreich (Academic, New York, 1969), Vol. 23, p. 1.
[10]M. S. Hybertsen and S. G. Louie, Phys. Rev. B **34**, 5390 (1986).
[11]R. W. Godby, M. Schlüter, and L. J. Sham, Phys. Rev. B **37**, 10 159 (1988).
[12]X. Zhu, S. B. Zhang, S. G. Louie, and M. L. Cohen, Phys. Rev. Lett. **63**, 2112 (1989) [GaAs(110)-(1×1)]; X. Zhu and S. G. Louie, Phys. Rev. B **43**, 12 146 (1991) [Ge(111)-(2×1)]; J. E. Northrup, M. S. Hybertsen, and S. G. Louie, Phys. Rev. Lett. **66**, 500 (1991) [Si(111)-(2×1)]; J. E. Northrup, Phys. Rev. B **47**, 10 032 (1993) [Si(100)-*c*(2×4)].
[13]M. S. Hybertsen and S. G. Louie, Phys. Rev. Lett. **58**, 1551 (1987) [As:Ge(111)]; Phys. Rev. B **38**, 4033 (1988) [As:Si(111)]; K. Hricovini, R. Günther, P. Thiry, A. Taleb-Ibrahimi, G. Indlekofer, J. E. Bonnet, P. Dumas, Y. Petroff, X. Blase, X. Zhu, S. G. Louie, Y. J. Chabal, and P. A. Thiry, Phys. Rev. Lett. **70**, 1992 (1993) [H:Si(111)].
[14]F. Aryasetiawan, Phys. Rev. B **46**, 13 051 (1992).
[15]E. L. Shirley and S. G. Louie, Phys. Rev. Lett. **71**, 133 (1993).
[16]W. von der Linden and P. Horsch, Phys. Rev. B **37**, 8351 (1988).
[17]R. Hott, Phys. Rev. B **44**, 1057 (1991).
[18]A. Baldereschi and E. Tosatti, Solid State Commun. **29**, 131 (1979).
[19]R. Car, E. Tosatti, S. Baroni, and S. Leelaprute, Phys. Rev. B **24**, 985 (1981).
[20]N. Hamada, M. Hwang, and A. J. Freeman, Phys. Rev. B **41**, 3620 (1990).
[21]D. L. Johnson, Phys. Rev. B **9**, 4475 (1974).
[22]M. S. Hybertsen and S. G. Louie, Phys. Rev. B **37**, 2733 (1988).
[23]X. Zhu and S. G. Louie, Phys. Rev. B **43**, 14 142 (1991).
[24]Z. H. Levine and S. G. Louie, Phys. Rev. B **25**, 6310 (1982).
[25]F. Bechstedt, R. Enderlein, and R. Wischnewski, Phys. Status Solidi B **107**, 637 (1981).
[26]C. Falter (private communication).
[27]C. Falter, M. Klenner, and W. Ludwig, Phys. Status Solidi B **167**, 85 (1991).
[28]M. S. Hybertsen and S. G. Louie, Phys. Rev. B **35**, 5585 (1987).
[29]G. B. Bachelet, D. R. Hamann, and M. Schlüter, Phys. Rev. B **26**, 4199 (1982).
[30]M. Sabisch (private communication).
[31]D. R. Hamann, M. Schlüter, and C. Chiang, Phys. Rev. Lett. **43**, 1494 (1979).
[32]D. M. Ceperley and B. I. Alder, Phys. Rev. Lett. **45**, 566 (1980).
[33]J. P. Perdew and A. Zunger, Phys. Rev. B **23**, 5048 (1981).
[34]D. J. Chadi and M. L. Cohen, Phys. Rev. B **8**, 5747 (1973).
[35]F. Gygi and A. Baldereschi, Phys. Rev. B **34**, 4405 (1986).
[36]*Numerical Data and Functional Relationships in Science and Technology,* edited by K.-H. Hellwege and O. Madelung, Landolt-Börnstein, New Series, Group III, Vols. 17a and 22a (Springer, Berlin, 1982).
[37]C. T. Chan, D. Vanderbilt, and S. G. Louie, Phys. Rev. B **33**, 2455 (1986).
[38]J. E. Ortega and F. J. Himpsel, Phys. Rev. B **47**, 2130 (1993).
[39]W. E. Spicer and R. C. Eden, in *Proceedings of the Ninth International Conference on the Physics of Semiconductors,* Moscow, 1968, edited by S. M. Ryvkin (Nauka, Leningrad, 1968), Vol. 1, p. 61.
[40]A. L. Wachs, T. Miller, T. C. Hsieh, A. P. Shapiro, and T.-C. Chiang, Phys. Rev. B **32**, 2326 (1985).
[41]F. J. Himpsel, P. Heimann, and D. E. Eastman, Phys. Rev. B **24**, 2003 (1981).
[42]R. Hulthen and N. G. Nilsson, Solid State Commun. **18**, 1341 (1976).
[43]D. Straub, L. Ley, and F. J. Himpsel, Phys. Rev. Lett. **54**, 142 (1985).
[44]See, e.g., *Solid State Physics, Advances in Research and Application* (Ref. 9), Secs. 11 and 25.
[45]E. L. Shirley, X. Zhu, and S. G. Louie, Phys. Rev. Lett. **69**, 2955 (1992).
[46]D. E. Aspnes, Phys. Rev. B **12**, 2297 (1975).
[47]D. Straub, L. Ley, and F. J. Himpsel, Phys. Rev. B **33**, 2607 (1986).
[48]F. J. Himpsel, J. F. van der Veen, and D. E. Eastman, Phys. Rev. B **22**, 1967 (1980).
[49]D. H. Rich, T. Miller, G. E. Franklin, and T.-C. Chiang, Phys. Rev. B **39**, 1438 (1989).
[50]T.-C. Chiang, R. Ludeke, M. Aono, G. Landgren, F. J. Himpsel, and D. E. Eastman, Phys. Rev. B **27**, 4770 (1983).
[51]T.-C. Chiang, J. A. Knapp, M. Aono, and D. E. Eastman, Phys. Rev. B **21**, 3513 (1980).
[52]S. Baroni and R. Resta, Phys. Rev. B **33**, 7017 (1986).